Orbits and photometry of Pluto's satellites: Charon, S/2005 P1 and S/2005 P2

Marc W. Buie, William M. Grundy

Lowell Observatory, 1400 W. Mars Hill Rd., Flagstaff, AZ 86001

buie@lowell.edu, grundy@lowell.edu

Eliot F. Young, Leslie A. Young, and S. Alan Stern

Southwest Research Institute, Boulder, CO

efy@boulder.swri.edu, layoung@boulder.swri.edu, alan@boulder.swri.edu

ABSTRACT

We present new astrometry of Pluto's three satellites from images taken of the Pluto system during 2002-3 with the High Resolution Camera (HRC) mode of the Advanced Camera for Surveys (ACS) instrument on the Hubble Space Telescope. The observations were designed to produce an albedo map of Pluto but they also contain images of Charon and the two recently discovered satellites, S/2005 P1 and S/2005 P2. Orbits fitted to all three satellites are co-planar and, for Charon and P2, have eccentricities consistent with zero. The orbit of the outermost satellite, P1, has a significant eccentricity of 0.0052 ± 0.0011. Orbital periods of P1, P2, and Charon are 38.2065 ± 0.0014, 24.8562 ± 00013, and 6.3872304 ± 0.0000011 days, respectively. The total system mass based on Charon's orbit is $1.4570 \pm 0.0009 \times 10^{22}$ kg. We confirm previous results that orbital periods are close to the ratio of 6:4:1 (P1:P2:Charon) indiciative of mean-motion resonances, but our results formally preclude precise integer period ratios. The orbits of P1 and P2, being about the barycenter rather than Pluto, enable us to measure the Charon/Pluto mass ratio as 0.1165 ± 0.0055. This new mass ratio implies a density of 1.66 ± 0.06 g cm^{-3} for Charon and 2.03 ± 0.06 g cm^{-3} for Pluto thus adding confirmation that Charon is somewhat under-dense relative to Pluto. Finally, by stacking all images, we can extract globally averaged photometry. P1 has a mean opposition magnitude of $V = 24.39 \pm 0.02$ and color of $(B - V) = 0.644 \pm 0.028$. P2 has a mean opposition magnitude of $V = 23.38 \pm 0.02$ and color of $(B - V) = 0.907 \pm 0.031$. The colors indicate that P1 is spectrally neutral and P2 is slightly more red than Pluto. The variation in surface color with radial distance from Pluto is quite striking (red, neutral, red, neutral) and begs further study.

Subject headings: astrometry, planets and satellites: individual (Pluto, Charon, S/2005 P1, S/2005 P2), Kuiper Belt

1.   Introduction

The study of Pluto was greatly facilitated in 1978 with the discovery of its first satellite, Charon (Christy and Harrington 1978). That discovery made possible the accurate determination of its mass which had previously been largely a matter of conjecture. Later, in the late 1980's, Pluto studies were transformed by the mutual events between Pluto and Charon (e.g., Buie et al. 1992; Binzel and Hubbard 1997; Young et al. 2001). Charon remains an interesting object it is own right, but its role as a tool from which to understand the system should not be understated.

Two new moons were recently discovered in orbit around Pluto (Weaver et al. 2005). More precisely, they orbit the center of mass of the system, which is very close to the Pluto-Charon barycenter. As with Charon, these new objects will be studied in their own right and will also be useful as probes or test masses in the Pluto system. Given astrometry of sufficient precision and time-base, one can now easily deduce the precise Charon/Pluto mass ratio. One might also hope to determine the masses of the new satellites through their mutual perturbations. However, their mutual gravitational force is more than 3 orders of magnitude weaker than the force exerted on them by Pluto and Charon, so the dynamics of their presumably resonant orbits may well completely mask any measurable effect P1 and P2 may have on each other.

The preliminary orbits computed by Weaver et al. (2005) were based on just two epochs of data separated by only three days, much less than a full orbit of either satellite. Also, the data were derived from images where Pluto and Charon were both saturated. These constraints led to a restricted solution for the orbit where it was assumed that the objects were in circular orbits in the same orbital plane as Charon. As we shall show, this assumption turned out to be very close to the correct answer.

The data presented in this work are derived from pre-discovery HST observations that span multiple orbits of all satellites and do so with images where Pluto and Charon are not saturated. This paper presents the first unrestricted fits to the orbits of the new satellites using pre-discovery HST observations.

2.   Observations

Images were taken of the Pluto system from June 2002 to June 2003 with the High Resolution Camera (HRC) mode of the Advanced Camera for Surveys (ACS) on the Hubble Space Telescope. The observations were designed to permit construction of a photometrically accurate map of the surface of Pluto. A total of 12 visits were allocated and scheduled to occur at specific sub-earth longitudes of Pluto at a 30-degree rotational resolution. The geometric circumstances of the observations are tabulated in Table 1. Each visit was designed to fit in a single visibility window but scheduling constraints stretched the time line out beyond a single orbit. Within each visit, two filters were used. F435W and F555W filters were chosen for their similarity to the standard

Johnson B and V bandpasses for which there is a substantial heritage of historical data on Pluto. The exposure times were chosen to give comparable signal levels on Charon (a neutrally colored object) but no attempt was made to adjust exposure times based on the lightcurve from Pluto. The signal level expected in the peak pixel on Pluto was roughly half of the full-well of the detector, leaving ample room to accommodate Pluto's lightcurve without saturating. All F435W exposures were 12 seconds and all F555W exposures were 6 seconds. Peak counts on Pluto ranged from 1900 – 3500 counts and Charon peak counts were from 700 – 2800 counts.

A total of 16 images were collected at each visit in each filter, using a customized dither pattern that provided a 4 by 4 sub-pixel grid superimposed on a 1.2 arcsec (48-pixel) pattern. This pattern was designed to enable the removal of both large and small scale pixellation effects in the image since the PSF of the telescope is undersampled by the HRC detector. The details of the dither pattern are not important for this project except to note distortion corrections are necessary during the processing of the data. If this is not done, the differential distortion in the dither set will lead to a slight blurring of the effective PSF in the co-added images. However, in some visits, the new satellites can be seen even without removing the differential distortion and this crude level of stacking was used for the confirmation alluded to in Weaver et al. (2005).

Two other important details about the data set should be noted. First, since the images span a full year, the data were collected at a range of solar phase angles, as well as various heliocentric and geocentric distances. The signal-to-noise ratio of object images in the data are clearly inversely proportional to distance and phase angle. Second, the data were collected with the largest possible range of roll angle from visit to visit. The first point led to an useful variation in parallax since the system was viewed from a slightly different orientation during each visit. The second point helped alleviate potential systematic effects from the geometric distortion and slightly asymmetric PSF inherent in the camera.

3. Analysis

The new satellites are not directly visible in individual data frames. Note that there are almost 10 stellar magnitudes difference in brightness between Pluto and the faintest satellite. To detect the satellites we had to co-register and co-add the images from a visit. When the data are stacked for each filter separately the objects are visible in many visits in each filter but the signal-to-noise ratio is low. To provide the best possible images for astrometric measurements we chose to co-add all 32 images (both filters) from each orbit into a single image for measurement.

As mentioned earlier and shown in Table 1, the duration of each visit was somewhat variable. The shortest visit did fit in a single visibility window and thus spans only 43 minutes from start to finish. The longest visit was spread over three visibility windows and spanned over 200 minutes. This time span leads to some smearing of the satellite images. The upper limit to this smearing is about three HRC pixels for the longest observational time span if it occurred at conjunction. In

practice, the amount of smear is smaller than this and depends on where in its orbit the satellite appears.

The focal plane of ACS not perpendicular to the optical axis, so a rectangle on the sky looks more like a rhombus in a raw HRC image. In the interest of preserving the maximum sensitivity on these faint objects we chose to implement our own method for removing the geometric distortion from the images by using the forward and inverse distortion coefficients[1] that were available from the STScI website and documented in Gonzaga et al. (2005).

To rectify the data, each individual image was resampled onto a rectilinear grid. To do this we used the inverse distortion coefficents to map pixel positions in an orthogonal grid back to CCD pixels in the HRC's skewed grid. We defined an undistorted grid with a platescale of 0.025"/pixel and a sub-sampling factor of 8 (virtual platescale of 0.003125"/pixel). The flux of each sub-sampled pixel was assigned the value from the distorted image where the position of the sub-sampled pixel is mapped. In this way the entire image on the sub-sampled grid is filled from values taken from the original image. Finally, the undistorted, subsampled images were rebinned to the final output platescale by averaging the flux in the 8 by 8 grid mapping to each output pixel.

Once the distortion was removed, the position of Charon was measured using a synthetic photometry aperture of 2.5-pixel radius and no attempt was made to correct for the variable PSF wing of Pluto at the position of Charon. A test fit was performed on the ACS-based astrometry for Charon to look for effects caused by PSF overlap. If present, the errors should show a double-peaked signature when phased by orbital longitude (maximum error at each minimum separation). This pattern was not seen and we conclude that the PSF-overlap errors are negligible compared to other sources of error in the astrometry.

The images were then stacked by nearest pixel registration based on Charon's position. Two sets of stacked images were produced, one was a straight sum of all frames and the other was a robust average (sigma-clipping algorithm) meant to suppress cosmic-ray strikes and other image imperfections. In the robust average the cores of Pluto and Charon do not stack properly and do not form useful images. Therefore, positions of Pluto and Charon were measured from the straight sum and positions of the faint satellites were measured from the robust average.

All raw positional measurements were made on undistorted frames that are rotated by some angle relative to the sky. We converted all raw measurements to a J2000 sky-plane measurement by rotating by the angle given in the ORIENTAT keyword in each image header. This rotation angle is held constant within a visit by the tracking procedure employed by HST. Any error in this angle is neglected though it will be included in the aggregate error during the fitting process since each visit has its own independent rotation. Additionally, all measurements are treated as

---

[1]More information about the reference files can be found at http://www.stsci.edu/hst/acs/analysis/reference_files/idc_tables.html. We used files n7o1634cj_idc.fits and n721640fj_idc.fits for observations made after 2002 Oct 21 or 2003 Mar 1, respectively.

relative measurements. The astrometric zero-point reference for each image provided in the image headers is not accurate enough for orbit fitting. The position of all four objects are accurate relative to each other within a frame. Charon was used throughout as a reference point from which the frame-relative measurements tied together into a single astrometric system.

We chose not to use Pluto as a registration object due to its larger and resolved size. Also, Pluto's substantially larger lightcurve amplitude relative to Charon (Buie et al. 1997) led us to use Charon to help minimize errors that might be introduced by center-of-light to center-of-body offsets.

The positions of Pluto, Charon, P1, and P2 were measured manually in the stacked images. The manual measurement was discretized at 1/10 pixel and done by drawing a 2.5-pixel radius circle on the image. When the circle was judged to be in the correct place based on a highly zoomed image with a logarithmic display stretch, the position was recorded. In the case of Pluto and Charon, the general location is quite obvious and the manual measurement can attempt to correct for systematic image effects (eg., overlapping PSFs).

Measuring P1 and P2 was also done with manual centering but identifying the region of interest is much more important. Analogous to moving object detection for Near-Earth object searches or Kuiper Belt surveys, having a geometric constraint enables identification of objects at a much lower signal-to-noise ratio via combining information from multiple epochs. The probability of a chance coincidence across visits that obeys a Keplerian orbit vanishes as the number of visits increases.

A crude predictor was used to identify where to look in the images. The first step was to draw projected ellipses on the image consistent with the discovery information (as found in IAUC 8625). The semi-major axes were used: $a_{P1} = 64700$ km and $a_{P2} = 49400$ km as well as the assumption of co-planar and circular orbits. From this guide we scanned the images for faint objects at any longitude near the projected ellipses of the orbits. Visit 7 showed the most convincing images of objects similar in brightness to that expected for P1 and P2. The reality of the detections was made even more convincing when the F435W and F555W images were stacked separately and the objects appeared in both filters. This detection formed the basis for our confirmation of the existence of P1 and P2 as reported in IAUC 8625 and Weaver et al. (2005).

Other images also showed possible detections. To check if these apparent detections were real, we considered whether their longitudes were consistent with possible Keplerian orbits. Starting from the initial orbital periods of the discovery report, we adjusted the periods so as to reproduce the positions of the satellites in Visits 1 and 7, arriving at 38.25 days for P1 and 24.85 days for P2. From this information we could crudely predict the locations of the satellites on all frames (stacked relative to Charon) and highlight a 10×10 pixel region of interest on those images. We then located and measured relative to Charon the position of the most convincing source within that region of interest. In all 12 visits a source was identified for P1 and sources were identified with P2 in 8 visits. These measurements, relative to Charon's location, formed the basis for our initial unrestricted orbital fits.

We also needed the position of Pluto, to estimate the location of the barycenter about which the satellites orbit. The centroid positions for Pluto were not used in the orbit fitting process to avoid using a center-of-light measurement. However, the primary purpose of this data set was to determine an albedo map for the surface of Pluto (Buie et al. 2005). This map allows for a more precise determination of the center of body during the map fitting process. A comparison of the two measurements shows a shift of 2 to 15 mas east and -10 to 17 mas in declination. We used the location of Pluto relative to Charon in conjunction with the Charon/Pluto mass ratio of 0.122 from Olkin et al. (2003) for an initial estimate of the location of the barycenter.

Orbits for P1 and P2 about the Olkin et al. (2003) barycenter were fitted using a downhill simplex minimization scheme (Nelder and Mead 1965), using code developed for fitting orbits of binary trans-neptunian objects (Noll et al. 2004a,b). Initial results from these fits looked very promising, with residuals mostly at or below a single HRC pixel (0.025 arcsec). At this step the measurements of P1 from visits 3 and 10 were excluded from the fit due to excessive residuals, 18 and 31σ respectively.

We expected that additional detections would be enabled by eliminating the differential smear between Charon and the new satellites. Our initial fitted orbits were used to predict the locations of P1 and P2 relative to Charon. From these positions, offsets were computed enabling us to stack the images on each satellite in turn, rather than stacking relative to Charon as was done before. In the resulting P1 and P2 stacked images, we identified sources for the satellites in all 12 visits. This second generation astrometry went into a second round of unrestricted orbit fits, again relative to the Olkin et al. (2003) barycenter. From the residuals relative to these new orbits it was apparent that one measurement of P2 and two of P1 had unacceptably large residuals and those measurements were removed from further consideration. At this point we had precise astrometric measurements of Pluto, Charon, P1, and P2, relative to one another. These data are tabulated in Table 2.

Next we fit completely unrestricted orbits to the data for Charon, P1, and P2. To extend the time baseline, and thus improve the constraint on the orbital periods, we included data from two additional sources. For Charon, 60 positions from Tholen and Buie (1997) were combined with our 394 positions (Charon was measurable in each individual frame, unlike P1 and P2 which could only be measured in the stacked images from each visit). For P1 and P2, our positions were augmented with the two Weaver et al. (2005) positions. In both cases, the additional data were collected with different observing strategies and different instruments, and thus have different potential systematic issues. For instance, the Tholen and Buie (1997) data were measured relative to the center of light of Pluto, not the center of body. Likewise the Weaver et al. (2005) positions were measured relative to the center of light of Pluto as deduced from its diffraction spikes, since Pluto itself was severely saturated.

Table 3 summarizes our best fit orbital elements. Orbital element uncertainties were estimated for each parameter by fixing the parameter in question at a series of values straddling the best value,

and for each of those values, allowing all other parameters to adjust themselves to re-minimize χ^2. This process produced a slice through χ^2 space. According to Press et al. (1992), $\chi^2_{\text{minimum}} + 1$ is the 1-σ confidence contour in this space, the location of which we report as an uncertainty. In instances of asymmetric χ^2 minima, we conservatively report the uncertainty computed for the shallower-sloped side of the valley.

We performed test fits restricted to just our new ACS astrometry for all three satellites. The only significant change seen in the orbit fits were larger errors on the periods. However, each orbit fit provides a measurement of the system mass when combining the period and semi-major axis. The fit to the combined data set for Charon gives $M_{\text{total}} = 1.4570 \pm 0.0009$ x 10^{22} kg and is the value we adopt for the remainder of this work. The mass inferred from the P1 orbit is 1.4765 ± 0.006 10^{22} kg and the mass from the P2 orbit is 1.480 ± 0.011 x 10^{22} kg. The P1- and P2-based masses agree with each other but do not completely agree with the Charon-based mass. So far we have been unable to explain this discrepancy and its resolution is left for future work.

4. Results

The projected orbits for Pluto, Charon, P1, and P2 are shown in Figure 1. Points with error bars show the sky plane positions of the observations while the open circles indicate the locations computed from our fitted orbits. The degree to which the circles are centered on the symbols indicates the quality of the fits. One can also see from this figure the effect of the changing geometry through the 12 months of observation, and especially for the Weaver et al. (2005) positions obtained 2 years later. The data (and the fitted orbit positions) do not exactly track the instantaneous apparent ellipse. This figure also shows that we managed to get reasonably complete longitude coverage of both new satellites.

Weaver et al. (2005) noted that the new satellites P1 and P2 orbit near mean motion resonances with Charon and with each other. Our improved orbit determinations confirm that the orbital periods are indeed near integer ratio commensurabilities. However, our uncertainties preclude the precise ratios for simple resonances. Determination of resonant motion will require a full description of the dynamical state of this four-body system using orbital integration calculations. These calculations are beyond the scope of this paper and remain for future work. Nonetheless, if these objects do inhabit resonances, the osculating elements must vary with time to maintain an oscillating resonant angle. A simple two-body calculation cannot reveal the nature of these mean-motion resonances nor can it determine the period of oscillations. We can use a two-body calculation to calculate the time for the resonant argument to circulate by 2π and thus provide a crude upper limit to the time-scale for the resonant libration.

The orbital period of P1 is 38.2065 ± 0.0014 days, while six times the period of Charon is 38.3234 days. While this is the period ratio most nearly commensurate, this 0.3% difference would lead to circulation of the resonant argument in 2090 ± 80 days, less than six years. Like-

wise, our period of P2 is 24.8562±0.0013 days, compared with 4 times the period of Charon, which is 25.5489 days, corresponding to a 2.7% difference, and thus the resonant argument will circulate in only 229±2days. Comparing the periods of P1 and P2, we find their ratio is 1.53710±0.00006, not the exact ratio of 3/2. Again, circulation would be quite rapid, 515±6 days. These timescales for resonant libration seem short but the mass distribution of this system is quite unusual. The dominant mass of Pluto+Charon can be viewed as if it were a highly asymmetric mass that provides a strong periodic driving force. The gravitational force exerted by Pluto on either P1 or P2 varies by roughly 15% (peak-to-peak). This periodic driving force may well control the nature of resonances in the system on an unusually short time-scale and certainly deserves further scrutiny.

Eccentricities and inclinations of the satellite orbits will offer important constraints on possible resonances. The eccentricity of the orbit of P1 (0.0052±0.0011) is significantly non-zero, unlike the orbits of Charon and P2 which are consistent with zero eccentricity. Figure 2 provides our best determination of the orbit poles, showing the 1-σ contours for the pole positions for the three satellites, as well as for the Charon orbit determined by Tholen and Buie (1997). The mild discrepancy between the two Charon poles may be an artifact of the lack of precise center-of-body measurements for Pluto in the earlier measurements. The same systematic offset can explain the apparently special alignment of the line of apsides in the orbit fitted to the earlier data as well as the apparent non-zero eccentricity of that orbit.

We note that every 35.57 days P1, P2, and the barycenter all line up, alternating between P1 and P2 both being on the same side of the barycenter versus being on opposite sides of it. This 35.57 day interval corresponds to one half of the difference of the mean motion of P1 and P2, and is does not require resonances among the satellites. Charon orbits much faster than P1 and P2, so the Charon-Pluto line sweeps across the P1-P2-barycenter line within a few days of each of P1-P2-barycenter alignment, providing opportunities when all four objects lie nearly along the same line. Depending on the date of its flyby of the Pluto system, New Horizons, NASA's first New Frontiers mission bound for Pluto and the Kuiper Belt (Stern and Cheng 2002), might be able to take advantage of one of these alignments to obtain an especially striking family portrait. The 35.57 day interval is shorter than the period of P1, so the orientation of each successive alignment shifts by about 27° in orbital longitude.

Figure 3 shows details of the residuals from the orbit fits for the HST data. The scatter for Charon is quite low in the fits but slightly better for our new data. The mean residual is 3.7 mas and maximum residual is 8 mas in our Cycle 11 data. The data from Tholen and Buie (1997) had a mean residual of 5 mas and a maximum residual of 11 mas. The lower panels of Figure 3 show the residuals for P1 and P2 on the same scale. The scatter is noticeably higher owing to the much lower signal-to-noise images but is still quite respectable, averaging about 9 mas for P1 and 17 mas for P2 (about half of a pixel). The Weaver et al. (2005) residuals (circled) are larger on average, owing to the lower spatial resolution of those measurements.

While fitting for each satellite's orbital elements, we also solved for the Charon/Pluto mass

ratio, which determines the location of the barycenter. Allowing the mass ratio to be a free parameter in these fits resulted in two independent mass ratio estimates, one from the orbit of P1 and one from the orbit of P2. The resulting χ^2 slices, converted to reduced χ^2 by dividing by the number of degrees of freedom, are shown in Figure 4. Our best determination comes from combining both fits with a resulting mass ratio of 0.1165±0.0055, consistent with the Olkin et al. (2003) value of 0.122±0.008. When combined with the new occultation diameter of Charon from Sicardy et al. (2005) of $R = 602.5 \pm 1.0$, we can now determine a much more accurate density for Charon of 1.66 ± 0.06 g cm^{-3} where the dominant source of error is the mass ratio. The density of Pluto is thus 2.03 ± 0.06 g cm^{-3} assuming a radius[2] of 1153 ± 10 km. The radius of Pluto is the dominant source of error and is also the most poorly understood due to the effects of the atmosphere on occultation lightcurves. Even with the relatively poor knowledge of Pluto's radius it is clear that Charon is significantly less dense than Pluto.

Each frame recorded insufficient signal from P1 and P2 to permit time-resolved photometry, but photometric information could be obtained by stacking all 192 images of each filter based on the orbital motion determined previously. The resulting stacked images are displayed in Fig. 5. We also stacked images and extracted globally averaged photometry from Pluto and Charon. The total aggregate integration time is 2304 and 1152 seconds for F435W and F555W, respectively.

Table 4 summarizes the photometric information extracted from the stacked images. Values listed without uncertainties are adopted from Buie et al. (1997). "OBMAG" is the instrumental magnitude using the same convention as Sirianni et al. (2005). The count rates shown for Pluto are provided as a rough guide to the signal level on the detector. Since Pluto is resolved in these data, our small-aperture fluxes cannot be easily corrected to reliable photometry. However, the aggregate PSF for Charon is nearly identical to that for P1 and P2. "OBMAG" is the instrumental magnitude derived from the count rates using the same convention as Sirianni et al. (2005). This raw photometry was converted to the $UBVRI$ system using the transformation coefficients of Sirianni et al. (2005). However, the aperture corrections required a non-standard method since the effective PSF was blurred by the stacking process. To correct for the small aperture we assumed the correction is the same for Charon, P1 and P2. The zero-point correction was determined by using the mean-opposition magnitude for Charon from Buie et al. (1997) of $V = 17.259$ and $(B - V) = 0.710$. "OppMag" refers to the transformed photometry that is relative to the mean opposition distance for Pluto's orbit ($r = 39.5$ AU, $\Delta = 38.5$ AU). Our new photometric data are a peculiar mix of information collected at a range of heliocentric and geocentric distances and solar phase angles. The signal-to-noise ratio in the P1 and P2 photometry is not good enough from single visits to permit extraction of any lightcurve or phase angle behavior. It is good enough to permit characterization of globally averaged properties since the geometries are exactly matched between

---

[2]Choosing a value for the radius of Pluto is not a simple matter. Current measurements from mutual events and stellar occultations do not completely agree and explanations of the discrepancies depend on the models chosen to interpret the data. Here we use the number adopted in most Pluto map fitting projects with an error bar chosen to include the range of model values for the radius from mutual event and stellar occultation data.

the three objects.

The lines listed as "AppMag" show the photometry corrected to the circumstances of the discovery of the two satellites as reported in Weaver et al. (2005, their photometry being listed as "Discovery"). The agreement in the P2 magnitude is excellent while our photometry of P1 is about 3-sigma fainter than previously reported. The agreement (or lack thereof) could easily be affected by lightcurve effects. If P1 has a large lightcurve we have measured the mean while the discovery observations could have been near a lightcurve maximum. A few tenths of a magnitude are not unreasonable for lightcurves of objects in this size range. The V magnitudes for P1 and P2 are almost identical, and correspond to 22 km radii, if the satellites' V albedos are similar to Charon's ($\sim$35%). The satellites would be larger if their albedos are lower than Charon's: 4% albedos correspond to $\sim$65 km radii.

The colors presented here indicate that P1 is a spectrally neutral object (solar colors within the uncertainties). This color might indicate a composition similar to Charon, although Charon is marginally redder. The color for P2 is slightly redder than Pluto. Both satellites exhibit colors which are common in the Kuiper Belt (e.g., Peixinho et al. 2004). The pattern with radial distance in the system is a bit harder to understand. If the colors of P1 and P2 were exogenic and derived from material lost from either Pluto or Charon it is hard to imagine P2 (the next one out from Charon) to be colored from Pluto material and not be expressed on Charon's surface. Likewise, P1 and P2 are not that far apart yet they have different colors. If these objects are collisional fragments of the Pluto-Charon binary formation process (Stern et al. 2005), the striking color difference may be hard to explain. These new observations also make it clear that environment alone cannot explain the color diversity amoung KBOs. Clearly, this is a profound mystery yet to be resolved.

5.   Acknowledgements

REFERENCES

Binzel, R.P., and Hubbard, W.B. 1997. In *Pluto and Charon*, University of Arizona Press, Tucson, pp. 85-102.

Buie, M.W., Tholen, D.J., and Horne, K. 1992. Icarus 97, 211.

Buie, M.W., Tholen, D.J., and Wasserman, L.H. 1997. Icarus 125, 233.

Buie, M.W. et al. 2005, BAAS 27, 4903.

Christy, J.W., and Harrington, R.S. 1978. AJ 83, 1005.

Gonzaga, S., et al. 2005, "ACS Instrument Handbook", Version 6.0, (Baltimore: STScI).

Olkin, C.B., Wasserman, L.H. and Franz, O.G. 2003. Icarus 164, 254.

Nelder, J., and Mead, R. 1965. Computer Journal 7, 308.

Noll, K.S., et al. 2004a. AJ 128, 2547.

Noll, K.S., et al. 2004b. Icarus 172, 402.

Peixinho, N., et al. 2004. Icarus 170, 153.

Press, W. H., et al. 1992. *Numerical Recipes in C: The Art of Scientific Computing*, Cambridge Univ. Press, New York.

Sicardy, B., et al. 2005. Bull. Amer. Astron. Soc. 37, 733.

Sirianni, M. et al. 2005. PASP, 117, 1049.

Stern, S. A. and Cheng, A. 2002. EOS, 83, 384.

Stern, S. A. et al. 2005. *Nature* in press.

Tholen, D.J., and Buie, M.W. 1997. Icarus 125, 245-260.

Weaver, H.A., et al. 2005. *Nature* in press.

Young, E.F., Binzel, R.P., and Crane, K. 2001. AJ 121, 552.

Table 1.   Circumstances of Observations

Midtime (JD)	Visit ID	r (AU)	Δ (AU)	α (degrees)	Δt (hours)
2452436.846680	1	30.518	29.521	0.36	1.71
2452440.051972	7	30.520	29.527	0.41	1.71
2452444.261280	3	30.521	29.539	0.50	1.74
2452458.083533	5	30.526	29.615	0.86	1.65
2452472.979577	9	30.532	29.751	1.24	1.66
2452550.688720	11	30.561	30.956	1.71	1.65
2452688.548688	6	30.613	30.944	1.73	0.70
2452750.256191	2	30.637	29.983	1.44	1.50
2452772.616060	8	30.646	29.757	0.91	1.49
2452787.606155	12	30.651	29.675	0.51	0.70
2452789.659917	4	30.652	29.668	0.46	1.71
2452799.257479	10	30.656	29.655	0.32	1.53

Note. — r and Δ are the heliocentric and geocentric distance to the Pluto-Charon barycenter. α is the Sun-barycenter-Earth (phase) angle. The visit ID is a number from the original observation sequence that is in order of increasing Pluto sub-Earth longitude and the time span from first to last image in a visit is listed under Δt.

Table 2.   Differential Astrometry

| Midtime | Visit | Charon | | S/2005 P1 | | S/2005 P2 | |
(JD)	ID	$\Delta\alpha$	$\Delta\delta$	$\Delta\alpha$	$\Delta\delta$	$\Delta\alpha$	$\Delta\delta$
2452436.846680	1	-0.4410	0.1192	1.5552	0.3647	0.9313	1.8835
2452440.051972	7	0.4501	-0.1106	1.6298	1.7786	0.1570	2.1420
2452444.261280	3	-0.4292	-0.6855	*0.7003*	*2.8137*	-1.0598	0.4708
2452458.083533	5	-0.0046	-0.8393	-1.6193	-1.4142	1.1989	0.1416
2452472.979577	9	0.4322	0.6662	1.3802	-0.5628	-1.0678	-1.3731
2452550.688720	11	0.0244	0.8020	1.4565	0.0808	*-0.4552*	*-2.0719*
2452688.548688	6	0.2570	-0.5580	-1.6226	-1.7965	0.1714	1.9567
2452750.256191	2	-0.5371	-0.2559	0.8133	2.8203	-0.3261	-2.1782
2452772.616060	8	0.5422	0.2580	0.0662	-2.6896	-0.9587	-1.9108
2452787.606155	12	-0.2843	0.5381	1.0365	2.8517	0.2195	2.2236
2452789.659917	4	-0.2797	-0.8646	0.5195	2.8330	-0.4735	1.6385
2452799.257479	10	0.2771	0.8657	*-1.6553*	*-0.0007*	-0.5006	-2.1083

Note. — The times for all measurements are the mean of the exposure mid-times for all combined images. All offsets are arcseconds in J2000 coordinates relative to the center of Pluto. Values in italics were not used in our orbit fits because of anomalously high residuals.

Table 3.   Orbital elements from unrestricted fits (epoch = 2452600.5)

	Charon	S/2005 P2	S/2005 P1
Period (days)	6.3872304(11)	24.8562(13)	38.2065(14)
Semi-major axis, a (km)	19,571.4(4.0)	48,675(121)	64,780(88)
Eccentricity, e	0.000000(70)	0.0023(21)	0.0052(11)
Inclination, i (deg)	96.145(14)	96.18(22)	96.36(12)
Lon. ascending node, Ω (deg)	223.046(14)	223.14(23)	223.173(86)
Lon. periapsis, $\tilde{\omega}$ (deg)	—	216(13)	200.1(3.7)
Mean lon. at epoch, l (deg)	257.946(13)	123.14(20)	322.71(23)

Table 4.   Photometry

		Pluto	Charon	S/2005 P1	S/2005 P2
photons/sec	F435W	4748.1 ± 1.5	1095 ± 0.7	1.641 ± 0.029	1.195 ± 0.025
	F555W	11136.3 ± 3.2	2101.8 ± 1.4	2.956 ± 0.055	2.765 ± 0.053
OBMAG	F435W	—	-7.599 ± 0.001	-0.538 ± 0.019	-0.193 ± 0.023
	F555W	—	-8.306 ± 0.001	-1.177 ± 0.020	-1.104 ± 0.021
OppMag	B_m	—	17.259	25.036 ± 0.019	25.357 ± 0.023
	V_m	—	17.969	24.393 ± 0.020	24.546 ± 0.021
AppMag	B	—	16.903	23.970 ± 0.019	24.291 ± 0.023
	V	—	16.193	23.327 ± 0.020	23.384 ± 0.021
	$(B-V)$	0.868	0.710	0.644 ± 0.028	0.907 ± 0.031
Discovery	V	—	—	22.93 ± 0.12	23.38 ± 0.17

Note. — Uncertainties are based on photon-counting statistics for the object and measured noise in the sky background. Scaling from instrumental to absolute magnitudes is done using the known mean magnitude for Charon from Buie et al. (1997). Magnitudes for Pluto are not reported due to indeterminant aperture corrections for a resolved object.

FIGURE CAPTIONS

Fig. 1.— Sky plane observations (points with error bars) and predicted positions (open circles) for P1 and P2, based on our best fit orbits. Observations of Charon are also shown, but the predicted positions are omitted to avoid clutter. Gray ellipses show the instantaneous orbits about the barycenter at a single, arbitrary epoch for Pluto, Charon, P2, and P1, from smallest to largest, respectively. The Weaver et al. (2005) measurements are distinguished by double circles for their predicted positions.

Fig. 2.— One sigma contours of orbit poles on the J2000 sky plane for our best fit orbits for Charon, P1, and P2, compared with the Tholen and Buie (1997) orbit pole for Charon ("TB97"). These contours were computed from a large set of orbits where each orbital element is drawn from a gaussian distribution consistent with the element and its associated uncertainties.

Fig. 3.— East-West and North-South residuals relative to our best fit orbits plotted versus orbital longitude for Charon (upper two panels, with open circles representing the 60 data points from Tholen and Buie (1997) and diamonds representing our 394 new observations) and for P1 and P2 (represented by asterisks and diamonds, respectively, in the lower two panels, with Weaver et al. (2005) data points circled).

Fig. 4.— Mass ratio slices in reduced χ^2 space for P1 and P2 (dashed and dotted curves, respectively), showing 1 sigma contours, defined as $\chi^2_{\mathrm{minimum}} + 1$ (Press et al. 1992). The solid curve is for P1 and P2 combined. The Olkin et al. (2003) mass ratio measurement is also indicated. The fact that reduced χ^2 levels are somewhat below unity suggests that our adopted astrometric uncertainties (± 0.009 arcsec for P1 and ± 0.015 arcsec for P2) are slightly too conservative.

Fig. 5.— Final stacked images for S/2005 P1 and P2. The left panels show the stacked images for the F435W filter. The right panels show the F555W filter data. The pair of images on the top are stacked based on the our fitted ephemeris motion for S/2005 P1 while the pair on the bottom were stacked on the S/2005 P2 ephemeris. The per-pixel sky noise is 0.3 e-/sec and is completely read-noise limited. The peak signals on the satelliates in each image are P1:F435W=2.93 e-/sec, P1:F555W=2.22 e-/sec, P2:F435W=1.89 e-/sec, and P2:F555W=2.19 e-/sec. The display stretch is the same for all four stacked images and is set to -3 to $+10\sigma$ of the sky level.
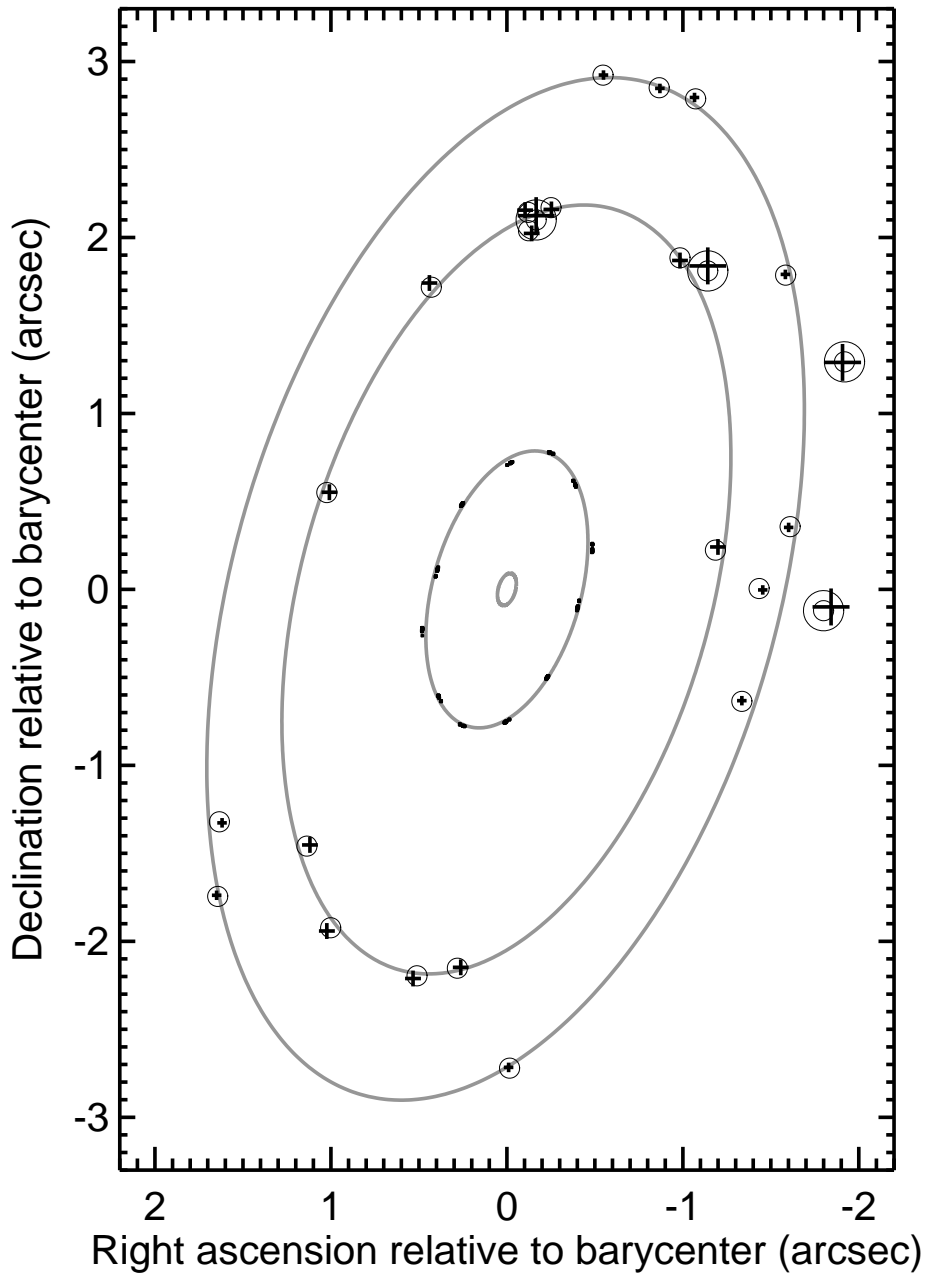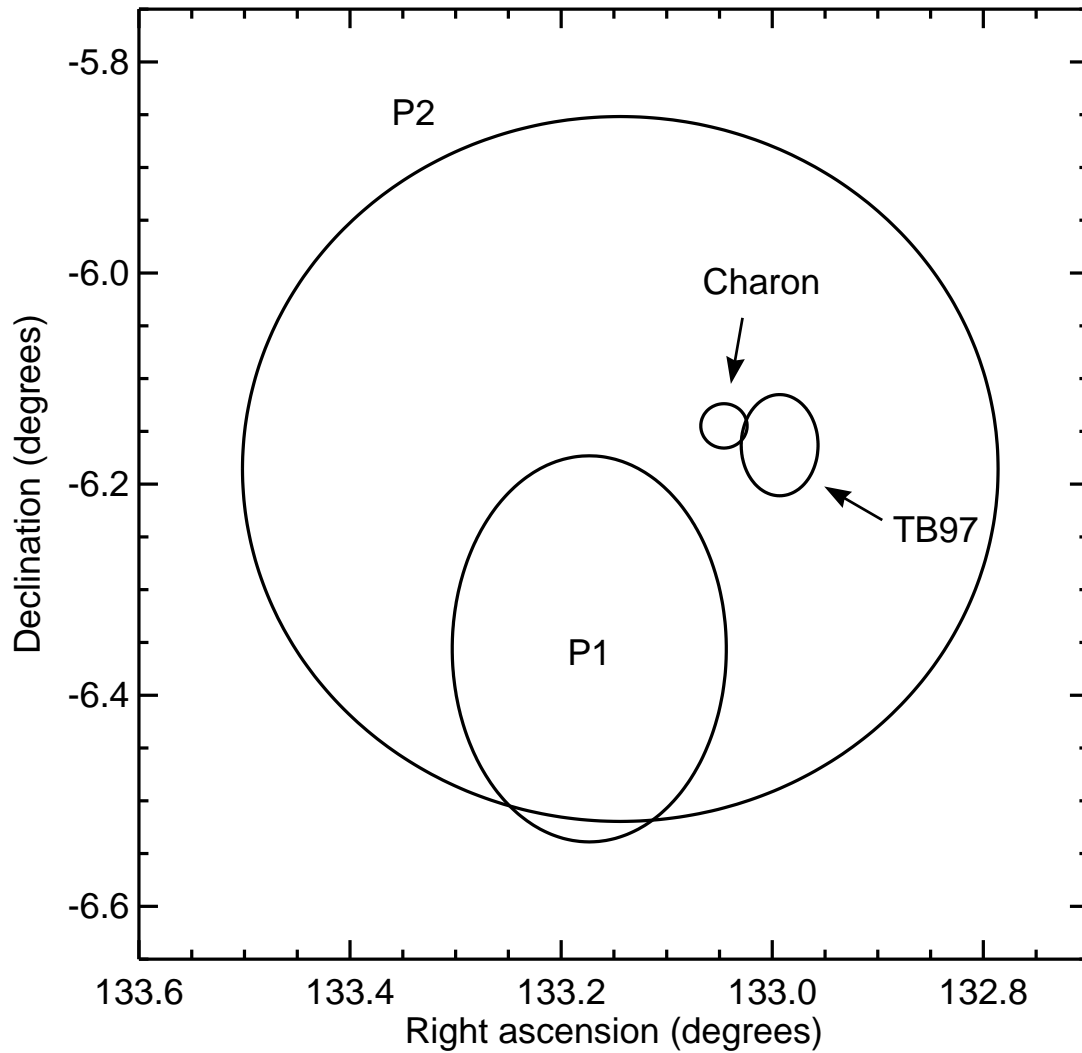
Fig. 1.— Sky plane observations (points with error bars) and predicted positions (open circles) for P1 and P2, based on our best fit orbits. Observations of Charon are also shown, but the predicted positions are omitted to avoid clutter. Gray ellipses show the instantaneous orbits about the barycenter at a single, arbitrary epoch for Pluto, Charon, P2, and P1, from smallest to largest, respectively. The Weaver et al. (2005) measurements are distinguished by double circles for their predicted positions.

Fig. 2.— One sigma contours of orbit poles on the J2000 sky plane for our best fit orbits for Charon, P1, and P2, compared with the Tholen and Buie (1997) orbit pole for Charon ("TB97"). These contours were computed from a large set of orbits where each orbital element is drawn from a gaussian distribution consistent with the element and its associated uncertainties.
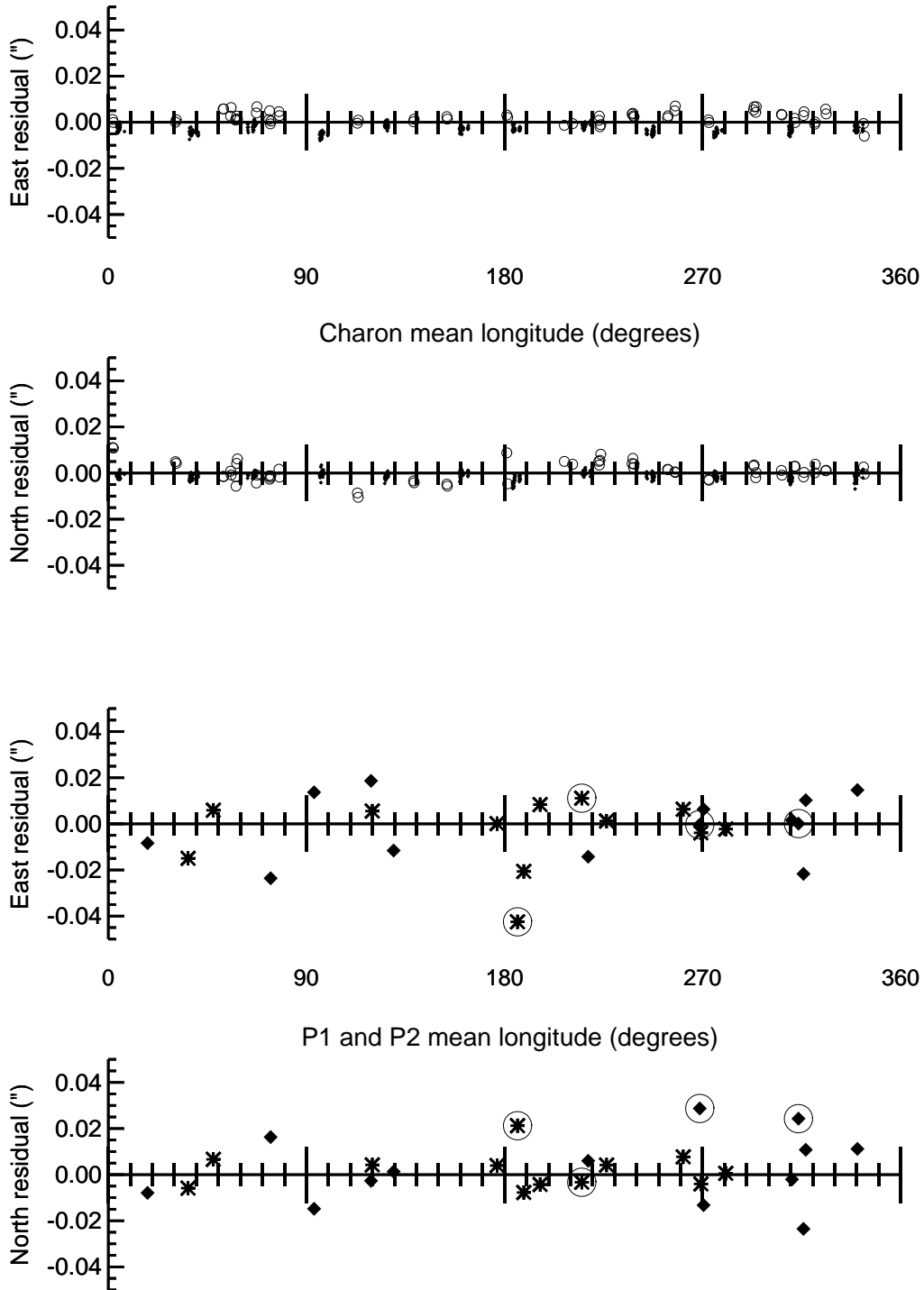
Fig. 3.— East-West and North-South residuals relative to our best fit orbits plotted versus orbital longitude for Charon (upper two panels, with open circles representing the 60 data points from Tholen and Buie (1997) and diamonds representing our 394 new observations) and for P1 and P2 (represented by asterisks and diamonds, respectively, in the lower two panels, with Weaver et al. (2005) data points circled).
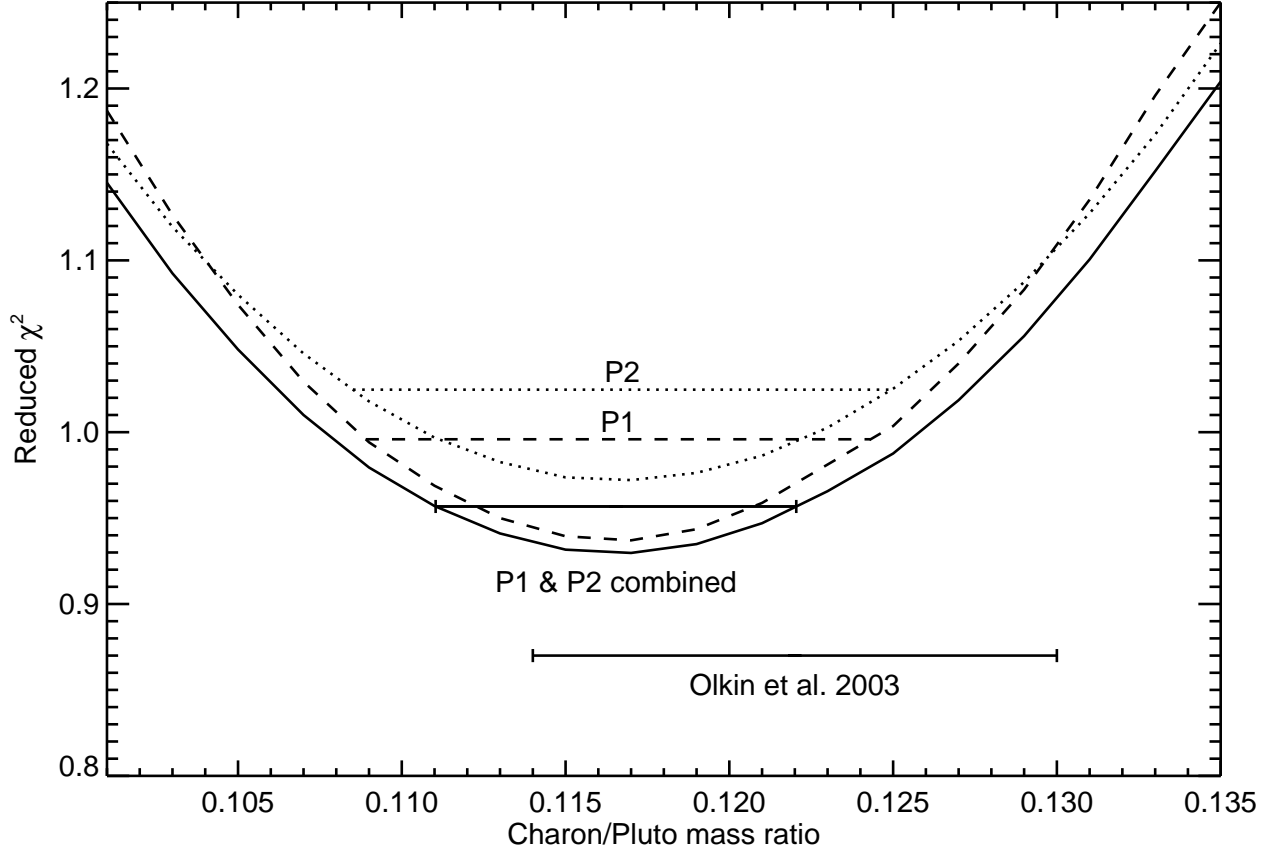
Fig. 4.— Mass ratio slices in reduced χ^2 space for P1 and P2 (dashed and dotted curves, respectively), showing 1 sigma contours, defined as $\chi^2_{\mathrm{minimum}} + 1$ (Press et al. 1992). The solid curve is for P1 and P2 combined. The Olkin et al. (2003) mass ratio measurement is also indicated. The fact that reduced χ^2 levels are somewhat below unity suggests that our adopted astrometric uncertainties (±0.009 arcsec for P1 and ±0.015 arcsec for P2) are slightly too conservative.
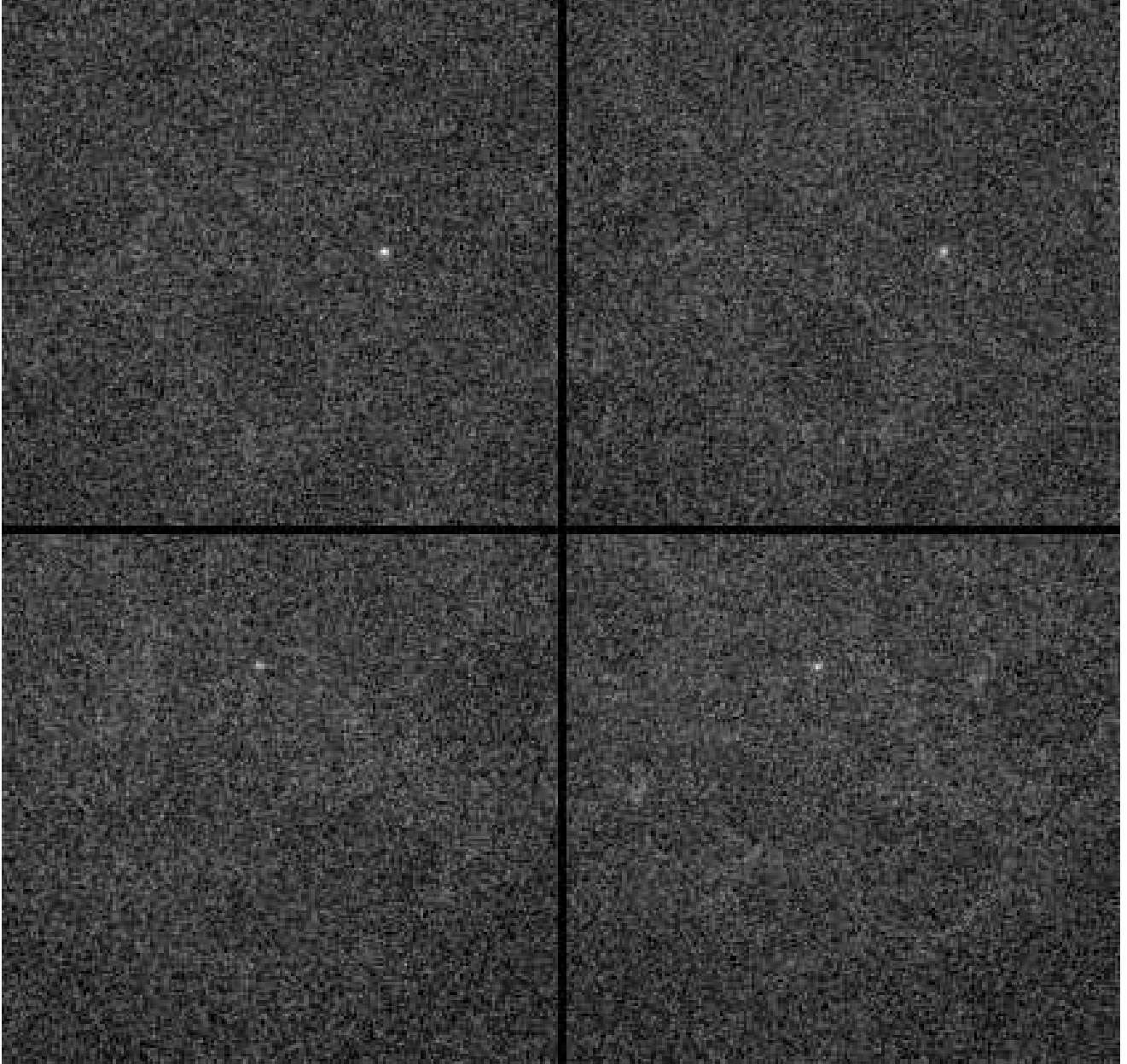
Fig. 5.— Final stacked images for S/2005 P1 and P2. The left panels show the stacked images for the F435W filter. The right panels show the F555W filter data. The pair of images on the top are stacked based on the our fitted ephemeris motion for S/2005 P1 while the pair on the bottom were stacked on the S/2005 P2 ephemeris. The per-pixel sky noise is 0.3 e-/sec and is completely read-noise limited. The peak signals on the satelliates in each image are P1:F435W=2.93 e-/sec, P1:F555W=2.22 e-/sec, P2:F435W=1.89 e-/sec, and P2:F555W=2.19 e-/sec. The display stretch is the same for all four stacked images and is set to −3 to +10σ of the sky level.